# A calibration-free electrode compensation method

Cyrille Rossant[1,2], Bertrand Fontaine[1,2], Anna K Magnusson[3,4], Romain Brette[1,2]

[1] Laboratoire Psychologie de la Perception, CNRS, Université Paris Descartes, Paris, France
[2] Equipe Audition, Département d'Etudes Cognitives, Ecole Normale Supérieure, Paris, France
[3] Center for Hearing and Communication Research, Karolinska Institutet, Stockholm, Sweden
[4] Department of Clinical Science, Intervention and Technology, Karolinska Institutet, Stockholm, Sweden

Running head: Calibration-free electrode compensation

Corresponding author: Romain Brette (romain.brette@ens.fr)

**Abstract**

In a single-electrode current clamp recording, the measured potential includes both the response of the membrane and that of the measuring electrode. The electrode response is traditionally removed using bridge balance, where the response of an ideal resistor representing the electrode is subtracted from the measurement. Because the electrode is not an ideal resistor, this procedure produces capacitive transients in response to fast or discontinuous currents. More sophisticated methods exist, but they all require a preliminary calibration phase, to estimate the properties of the electrode. If these properties change after calibration, the measurements are corrupted. We propose a compensation method that does not require preliminary calibration. Measurements are compensated offline, by fitting a model of the neuron and electrode to the trace and subtracting the predicted electrode response. The error criterion is designed to avoid the distortion of compensated traces by spikes. The technique allows electrode properties to be tracked over time, and can be extended to arbitrary models of electrode and neuron. We demonstrate the method using biophysical models and whole cell recordings in cortical and brainstem neurons.

Keywords:

- electrode compensation
- intracellular recording
- patch clamp
- current clamp

# Introduction

Intracellular recordings in slices have been used for decades to probe the electrical properties of neurons (Brette et Destexhe, 2012). These recordings are done using either sharp microelectrodes or patch electrodes in the whole cell configuration. In both cases, when a single electrode is used to pass the current and to measure the potential, the measurement is biased by the electrode. As a first approximation, the electrode can be modeled as a resistor (resistance $R_e$). Thus the measurement is the sum of the membrane potential and of the voltage across the electrode, which, by Ohm's law, is $R_e.I$ for a constant injected current I (in the current-clamp configuration). Therefore, the distortion due to the electrode can be significant when the electrode resistance is high compared to the membrane resistance. Sharp microelectrodes have a thin tip and therefore a high resistance (Purves, 1981). The resistance of patch electrodes is usually lower, since the tip is wider, but it may be high in some situations, for example *in vivo* (Anderson et al., 2000; Wehr et Zador, 2003) or in dendrites (Davie et al., 2006; Angelo et al., 2007) and axons (Shu et al., 2007). Perforated patch clamp recordings, in which the membrane is perforated by antibiotics in the electrode solution to avoid cell dialysis, also have high access resistance. Low resistance electrodes are also an issue in cells with low membrane resistance. Finally, in very long patch recordings with low resistance electrodes, the electrode often clogs up with time, which increases the resistance.

Thus it is often necessary to compensate for the electrode bias in single electrode recordings. The standard compensation technique is bridge balance, and is generally done directly on the electrophysiological amplifier. It consists in subtracting $R_e.I$ from the uncompensated recording, where $R_e$ is the estimated electrode resistance (usually manually adjusted using the response to current pulses). There are two issues with this method. First, even if $R_e$ can be accurately estimated, the electrode is not a pure resistor: it has a non-zero response time, due to capacitive components. This produces artifacts in the compensated trace, as shown in Figure 1. When a current pulse is injected (top left), the bridge model over-compensates the trace at the onset of the pulse, resulting in capacitive transients of amplitude $R_e.I$ (Fig. 1, middle left). These transients become an issue when fast time-varying currents are injected, such as simulated synaptic inputs (Fig. 1, top right). In this case, capacitive transients distort the compensated trace, which may even make the detection of action potentials difficult (Fig. 1, middle right). The second issue is that the capacitive component of the electrode can make the estimation of $R_e$ difficult, given that $R_e$ cannot be estimated in the bath (it changes after impalement).

A recent technique solves this problem by calibrating a model of the electrode using white noise current (Brette et al., 2008). However, as with other methods, the recordings may be corrupted if electrode properties change after calibration. To address this issue, we propose a model-based method to compensate current clamp recordings, which does not require preliminary calibration. Instead, the electrode model is fitted offline, using the recorded responses to the injected currents, with a special error criterion to deal with neuron nonlinearities and spikes. An example of compensated trace is shown in Fig. 1 (bottom). The technique is demonstrated with biophysical neuron models and current clamp recordings of cortical and brainstem neurons. We also propose quantitative tests to evaluate the quality of recordings.

# Methods

## Experimental preparation and recordings

We recorded from pyramidal cells in slices of the primary auditory cortex of mice (aged P9-15), at room temperature (25 ± 2°C), as detailed in (Rossant et al., 2011c). In addition, we recorded from the ventral cochlear nucleus in mice brainstem slices (aged P10). The principal cells of the cochlear nucleus were identified based on their voltage responses to de- and hyperpolarizing current pulses (Fujino et Oertel, 2001). Whole-cell current-clamp recordings were done with a Multiclamp 700B amplifier (Axon Instruments, Foster City, CA, U.S.A) using borosilicate glass microelectrodes with a final tip resistance of 5–10 MΩ. The pipette capacitance compensation was applied by using the amplifier's circuits, but we did not apply bridge balance on the amplifier. The signals were filtered with a low-pass 4-pole Bessel filter at 10 kHz, sampled at 20 kHz and digitized using a Digidata 1422A interface (Axon Instruments, Foster City, CA, U.S.A). In order to test that the electrode compensation method correctly distinguishes electrode and neuron resistance (Fig. 5), we increased the neuron's input resistance by applying the h-current blocker ZD7288 (10µM) to the slice bath. A small–moderate blockade of Ih, which is a large contributor of the input resistance of all cells in the ventral cochlear nucleus (Cao et Oertel, 2011), gave rise to significant increases of the input resistance without affecting the spiking properties.

## Electrode compensation

We consider a linear model of the neuron and electrode. Each element is modeled as a resistor + capacitor circuit (see Fig. 2A). The equations are:

$$\tau_m \frac{dV_{neuron}(t)}{dt} = V_r - V_n(t) + RI_{inj}(t)$$

$$\tau_e \frac{dV_{model}(t)}{dt} = R_e(I(t) - I_{inj}(t))$$

$$I_{inj} = (V_{model} - V_{neuron}) / R_e$$

$$U_e = V_{model} - V_{neuron}$$

where $V_{neuron}$ is the membrane potential of the neuron, $U_e$ is the voltage across the electrode, $\tau_m$ and $\tau_e$ are the membrane and electrode time constants, R and $R_e$ are the membrane and electrode resistance, and $V_r$ is resting potential. The 5 parameters are adjusted to minimize the $L^p$ error between the model prediction $V_{model}$ and the raw (uncompensated) measured trace $V_{raw}$:

$$e_p = (\int |V_{model}(t) - V_{raw}(t)|^p)^{1/p}$$

where p is a parameter (p = 0.5 is a good choice). After optimization, the compensated membrane potential of the cell is $V_{raw} - U_e$.

To perform the optimization, we use the downhill simplex algorithm (implemented as function *fmin* in the Scipy numerical library for Python). Since the equations are linear, the model prediction is computed by applying a two-dimensional linear filter to the injected current (see

Appendix). Although we used the simple model above in this paper, it may be replaced by more complex models by simply specifying the model equations in our tool. The corresponding linear filter is automatically calculated from the differential equations of the model (see Appendix). For the case when the equations are not linear, we also implemented a more complex method using a generic model fitting toolbox (Rossant et al., 2011b), based on the Brian simulator (Goodman et Brette, 2009) for the model simulation, and on the parallel computing library Playdoh (Rossant et al., 2011a) for the optimization. Initial parameters for the optimization can be selected by the user. A good practice is to use the estimated parameters for the initial part of a recording as initial parameters for the subsequent part.

The electrode compensation software is freely available as part of the Brian simulator (http://briansimulator.org).

**Currents**

We injected three different types of time-varying currents.

*Filtered noise.* This is a low-pass filtered noise (Ornstein-Uhlenbeck process) with 10 ms time constant.

*Current A.* This corresponds to current A in (Rossant et al., 2011c). It is a sum of a background noise and exponentially decaying post-synaptic currents (PSCs). The background noise is an Ornstein-Uhlenbeck process (i.e., low-pass filtered white noise) with time constant $\tau_N$=10 ms. The PSCs occur every 100 ms with random size: $PSC(t)=\alpha w e^{-t/\tau_s}$, where $\tau_s$ = 3 ms, $\alpha$=665 pA is a scaling factor, and w is a random number between 0.04 and 1.

*Current B.* This corresponds to current B in (Rossant et al., 2011c). It is a sum of random excitatory and inhibitory PSCs (with time constants $\tau_e$=3 ms and $\tau_i$=10 ms, respectively) with Poisson statistics, in which "synchrony events" are included. These events occur randomly with rate $\lambda_c$, and for each event we pick *p* excitatory synapses at random and make them simultaneously fire.

**Biophysical model**

In Figure 3, we tested the compensation method in a model consisting of a neuron and an electrode. The electrode is modeled as a resistor + capacitor circuit. The neuron model is a biophysical single-compartment model of a type 1-c neuron of the ventral cochlear nucleus, as described in (Rothman et Manis, 2003). The same model is used in Fig. 5A.

We used three sets of currents. Set 1 is a filtered noise, which makes the neuron fire at 1-5 Hz. Set 2 is current B with p = 15 and $\lambda_c$ = 5 Hz, which makes the neuron fire at 5-7 Hz. Set 3 is the same as set 2, but scaled to make the neuron fire at 15-20 Hz.

**Spike detection**

To detect spikes in compensated traces (Fig. 6), we first detect all times at which dV/dt changes sign, and register the value of V at these times. We build a histogram of these values (20 bins in

our recordings) and split it in two modes according to a decision threshold that is automatically determined as follows. We first discard all values below the median to increase robustness. We then look at local minima in the histogram. If there is none, the middle between the median and the highest value is taken as the decision threshold. If there is only one, it is chosen as the decision threshold. If there are two or more, the detection threshold is either the middle of the longest sequence of identical local minima, or the smallest local minimum. More sophisticated clustering methods could also be used but this simple approach proved sufficient for our recordings.

Voltage values in the histogram are considered as spike peaks when their voltage is greater than the decision threshold. Spike detection quality can be directly assessed from the separation of the two modes, using signal detection theory. Assuming that the two modes are normally distributed, we can calculate the probability that a spike peak is successfully detected (true positive), and the probability that a subthreshold peak is mistakenly classified as a spike peak (false positive), according to the following equations:

$$TP/P = 1 - \Phi\left(\frac{V_s - \mu_2}{\sigma_2}\right)$$

$$FP/N = 1 - \Phi\left(\frac{V_s - \mu_1}{\sigma_1}\right)$$

where TP/P and FP/N are the true and false positive rates, $\Phi(v) = \frac{1}{\sqrt{2\pi}}\int_{-\infty}^{v} e^{-x^2/2}dx$ is the cumulative distribution function of a Gaussian distribution, $V_s$ is the detection threshold, and $\mu_1$, $\mu_2$, $\sigma_1$, $\sigma_2$ are the parameters of the two distributions. Spike detection is reliable when TP/P is close to 1 and FP /N is close to 0.

**Quality coefficient**

A quality coefficient is calculated to assess the quality of electrode compensation, based on the idea that the voltage at spike peak should not depend on the current injected after spike initiation (Fig. 8). First, we try to predict the voltage at spike peaks based on the voltage before spike initiation. For each spike, a linear regression is performed on the compensated trace in a temporal window from 10 ms to 2 ms before spike peak. We then compute the best linear prediction of the spike peak, given the two regression parameters (intercept and slope). The quality coefficient is defined as the Pearson correlation between the prediction error and the mean input current around spike peak (2 ms before to 1 ms after).

**Two-compartment model**

In Fig. 9, we simulated a pyramidal neuron model with two compartments representing the soma and dendrites (Wang, 1998), with a filtered noisy current injected at the soma. The electrode is modeled as an RC circuit with $R_e$=200 MΩ and $\tau_e$=0.2 ms. In Fig. 9B, the model used for compensation also has a dendritic current, following the electrical circuit shown in the figure.

### Adaptive threshold model

In Fig.10E-G, we used an exponential integrate-and-fire neuron model (Fourcaud-Trocme et al., 2003) with adaptive threshold, as described in (Platkiewicz et Brette, 2010a, 2011a). The membrane equation describing the dynamics of the membrane potential V contains a leak current and an exponential approximation of the sodium current:

$$\tau_m \frac{dV}{dt} = (E_l - V_m) + \Delta \exp\left(\frac{V-\theta}{\Delta}\right) + R_m I$$

where $\tau_m = 5ms$ is the membrane time constant, $E_l = -70mV$ is the leak reversal potential, $\Delta = 1mV$ characterizes the sharpness of spike initiation, $R_m = 100M\Omega$ is the membrane resistance and $I$ is the injected current. The voltage diverges quickly to infinity once it exceeds the dynamic threshold $\theta$, which adapts to V through the following equation, based on an analysis of sodium inactivation dynamics in Hodgkin-Huxley models:

$$\tau \frac{d\theta(t)}{dt} = \theta_\infty(V) - \theta(t)$$

where $\theta_\infty(V) = V_T - k_a \log h_\infty(V)$ is the steady-state threshold, determined by $V_T = -67mV$, the minimum threshold, $k_a = 4.3mV$ is the Boltzmann factor of the sodium activation function, and $h_\infty$ is the inactivation function:

$$h_\infty(V) = \frac{1}{1+\exp\left(\frac{V-V_i}{k_i}\right)}$$

where $V_i = -69mV$ is the half-inactivation voltage of sodium channels. These values ensure that the spike threshold is variable (Platkiewicz et Brette, 2011a).

## Results

*Principle*

The principle is illustrated in Fig. 2A. A time-varying current is injected into the neuron and the raw (uncompensated) response (neuron + electrode) is recorded. We try to predict this response with a model including both the neuron and electrode. We used a simple linear model for both elements (resistor + capacitor), but it could be replaced by any parametric model. We calculate the prediction error, and we adjust the model parameters so as to reduce the error. The process is iterated until the error is minimized. When the model trace is optimally fitted to the raw recorded trace, we subtract the predicted electrode voltage from the raw trace to obtain the compensated trace.

Fig. 2B shows an example of successful compensation. The optimized model trace (left, solid)

tracks the measured trace (gray), but not with perfect accuracy. In particular, the action potential is not predicted by the model, which was expected since the model is linear. This is not a problem since we are only interested in correctly predicting the electrode response, which is assumed to be linear, in order to subtract it from the raw trace. Therefore it is not important to predict neuronal nonlinearities, as long as they do not interfere with the estimation of the electrode response. Fig. 2B (right) shows the compensated trace, which is the raw trace minus the electrode part of the model response.

However, neuronal nonlinearities, for example action potentials, may interfere with the estimation of the electrode model, as is illustrated in Fig. 2C. Here the neuron fired at a higher rate. The model parameters are adjusted to minimize the mean squared error between the model trace and the raw trace (left). To account for spikes, the linear model overestimates the electrode response (left, inset). As a result, the compensated trace is heavily distorted (right traces). The distribution of the difference between raw trace and model trace ($V_{raw}$-$V_{model}$) is shown on the right. The mean is zero, by construction, because the model minimizes the mean squared error. But the histogram peaks at a negative value, which means that most of the time, the model overestimates the raw trace. This is balanced by a long positive tail due to the spikes.

To solve this problem, we replace the mean square error by a different criterion which reduces the influence of this long tail, that is, of "outliers". Instead of minimizing the mean of $(V_{raw}-V_{model})^2$, we minimize the mean of $|V_{raw}-V_{model}|^p$, where $p<2$. This is called the $L^p$ error criterion. In this way, the error is compressed so that large deviations (action potentials) contribute less to the total error. The result is shown in Fig. 2D with $p=0.5$. The compensated trace is now much less distorted and the distribution of differences between model and raw traces peaks near zero.

*Validation with a biophysical model*

We first test the method using a biophysical neuron model, together with a resistor-capacitor model of the electrode (Fig. 3). To evaluate our method in a challenging situation, we used a highly nonlinear single-compartment model of cochlear nucleus neurons (Rothman et Manis, 2003), which includes several types of potassium channels. This biophysical model is used to generate the raw traces, but not to compensate them. That is, we still fit a simple linear model to the raw traces. The electrode time constant was $\tau_e$ =0.1 ms, compared to a membrane time constant of about 5 ms.

We injected fluctuating currents (see Methods) into the electrode (Fig. 3A, top), consisting of a mixture of background filtered noise and large random postsynaptic currents (PSCs). Here the neuron and electrode resistances were comparable (about 500 MΩ), and therefore the uncompensated recording was highly corrupted by the electrode (middle, gray). The solid trace shows the fit of the linear model to the raw trace (with $p = 0.5$). Once the electrode part of the linear model is subtracted, the compensated trace is hardly distinguishable of the true membrane potential of the biophysical neuron model (bottom).

We varied the electrode resistance $R_e$ between 50 and 500 MΩ, and tested the compensation technique with three different types of currents, to vary the output firing rate of the neuron (between 1 and 20 Hz). In all cases, the electrode resistance was very well estimated by the method (Fig. 3B). We then tested the influence of the error criterion (Fig. 3C). Using the mean

squared error (p = 2) clearly gave inferior results, even when the cell spiked at low rate. This is presumably because the neuron was highly nonlinear, which perturbed the estimation of the electrode. Best results were obtained with $p \leq 0.5$, with no significant improvement below p=0.5. Noise in real recordings could degrade performance for very low values of p, and therefore we suggest to use p=0.5 in general.

*Compensation of cortical recordings*

We then injected fluctuating currents with large transients into cortical neurons *in vitro* (pyramidal cells of the mouse auditory cortex), using high resistance patch electrodes. Because of these transients, raw traces were noisy and spikes could not be clearly distinguished (Fig. 4A, top). After compensation, traces were smoother and spikes stood out very clearly (bottom).

One advantage of this technique is that electrode properties can be tracked over the time course of the recording. In Fig. 4B, we show the evolution of the neuron and electrode resistance, as estimated by the model, during 10 minutes of recording (fluctuating current was injected). The recording was divided in slices of one second, and each slice was independently compensated (by running the model optimization on every slice). First, we observe some variability in the neuron resistance, but little variability in the estimated electrode resistance (at least for the first 5 minutes). This is a sign of a good electrode compensation, because electrode properties should be stable on a short time scale, while the properties of the neuron should change during stimulation, as ionic channels open and close. Quantitatively, the standard deviation of the estimated $R_e$ in the first 5 minutes is $\sigma_e = 11.6$ MΩ. Given that the mean current is $\mu_I = 20$ pA, the error in membrane potential estimation should be of order $\mu_I.\sigma_e = 0.23$ mV.

Second, in the middle of the recording, we observe that the electrode resistance slowly increases. This is unlikely to be an artifact of our compensation technique, because the neuron resistance remains stable and the estimated electrode resistance is also stable on shorter time scales. It could be for example because the electrode moved. This is an example where this technique is especially useful, because the recordings can still be compensated even though electrode properties change, as illustrated in Fig. 4C. On the left, a compensated trace (solid) is shown superimposed on the raw trace (gray), at the beginning of the recording (1). The same is shown on the right at the end of the recording (2), with updated electrode parameters. The raw trace is now further away from the compensated trace, because the electrode resistance has increased. If the electrode parameters are not updated, that is, we use the electrode properties obtained at the beginning of the recording to compensate the end of the recording, then the compensated trace is significantly different (bottom right): in particular, what looked like a post-synaptic potential preceding the spike now looks like a "spikelet", which is presumably a residual electrode response to an injected post-synaptic current.

To check that the technique indeed correctly tracks changes in electrode resistance, we simulated an abrupt change in $R_e$ in a model recording, in which the neuron receives a fluctuating current (Fig. 5A). In the middle of the recording, $R_e$ increases from 100 MΩ to 300 MΩ (dashed step). The method correctly tracks this change, while the estimate of the membrane resistance R is unchanged. To check that changes in neuron properties do not perturb the method, we injected a filtered noise current in a neuron of the cochlear nucleus and we

pharmacologically increased the membrane resistance (Fig. 5B). These neurons strongly express a hyperpolarization-activated current named Ih (Cao et Oertel, 2011). From the middle of the experiment, we apply an Ih blocker (see Methods). As expected, the estimated neuron's resistance increases sharply, while the estimated electrode resistance remains stable.

*Spike detection*

The simplest application of the method is to reliably detect spikes in current-clamp recordings. We now describe a spike detection procedure, in which the rate of errors can be evaluated (Fig. 6). Although we developed it for the present compensation technique, it could be applied in principle to any compensated recording. The procedure relies on the observation that when the recordings are plotted in phase space (dV/dt vs. V, Fig. 6A), spike peaks appear as crossings of the line dV/dt = 0 at high values of V. In a correctly compensated recording, these crossings are clearly distinct from those corresponding to subthreshold fluctuations (low values of V). Our procedure consists in computing a histogram of crossing values (Fig. 6B) and splitting it into two modes by choosing an appropriate decision threshold (see Methods). Crossings above the decision threshold are considered as spike peaks (Fig. 6C). The quality of spike detection can then be estimated with signal detection theory as follows. We approximate the two modes of the histogram as normal distributions. The probability that a sample from the subthreshold distribution exceeds the decision threshold is the false alarm rate, while the probability that a sample from suprathreshold distribution exceeds the decision threshold is the hit rate. In the specific recording shown in Fig. 6, the distributions were very well separated, so the hit rate was near 100% and the false alarm rate was near 0%.

*Quality and stability of electrode compensation*

The temporal stability of the estimated electrode resistance may also be used as a quality check of the compensation. To check this point, we simulated the response of a biophysical neuron model with an electrode (same as in Fig. 3) to a filtered noisy current. We then estimated the electrode and neuron resistances in each 1 s slice of a 1 minute recording (Fig. 7A). The results are very similar to Fig. 4B: the neuron resistance is quite variable while the electrode resistance is very stable. The estimation of $R_e$ varied by about 10% (standard deviation/mean - two outliers ($R_e$ > 400 MΩ) were removed), while the true value was within 5% of the mean (200 MΩ vs. 192 MΩ).

In a single-electrode recording, it is difficult to do an independent check of the quality of electrode compensation. Nevertheless, we suggest a simple test based on action potential shape. The shape of action potentials can vary (slightly) over time in a single cell, in particular the spike threshold and peak value (Platkiewicz et Brette, 2010a). However, these changes tend be coordinated, for example spikes with a low onset tend to have a higher peak. Fig. 7B (top left) shows an example of this phenomenon in a neuron of the prefrontal cortex *in vivo* (Léger et al., 2005). This may be explained by sodium inactivation (Platkiewicz et Brette, 2011a): at lower membrane potentials, sodium channels are less inactivated, and therefore more sodium current enters the cell, which produces higher spikes. It is useful to represent spikes in a phase space, where the derivative of the membrane potential Vm (dVm/dt) is plotted against Vm (Fig. 7B, top

right). In this representation, spikes form concentric trajectories that do not cross each other.

We found the same phenomenon in compensated traces of our *in vitro* recordings (Fig. 7B, middle). How would the traces look like in phase space if the electrode resistance were misestimated? It should result in random shifts of the membrane potential (essentially proportional to the current injected at spike time) and therefore in random shifts of the spike trajectories in phase space along the horizontal direction. This horizontal jitter should make some trajectories intersect. This is indeed what happens in Fig. 7B (bottom), where we compensated the recording with an electrode resistance mistuned by 25%. Therefore, in this case, we may be relatively confident that $R_e$ was estimated with at least 25% accuracy.

We developed a more quantitative test of compensation quality based on spike shape (Fig. 8). It is based on the idea that the voltage at spike peak should not depend on the current injected after spike initiation. In a previous study, Anderson et al. (2000) used a similar principle to estimate the electrode resistance: if the voltage value at spike peak is constant, then the correlation between the measured voltage at spike peak and the injected current is precisely the residual (non-compensated) electrode resistance. The interest of this estimation method is that it only uses information based on spike shape, while other estimation methods (including ours) uses only information in the subthreshold response. Therefore it can be seen as an independent control. One weakness of this method is that the voltage at spike peaks is in fact not constant and depends on membrane potential history, as we previously mentioned. This can introduce spurious correlations between injected current and spike peak voltage, which are not indicative of poor electrode compensation. We refined this method to address this issue (Fig. 8A and Methods). First, we predict the spike peak from the membrane potential preceding the spike, using a linear regression to the preceding voltage. Second, we calculate the Pearson correlation between the current injected during the spike and the error in predicting the peak value. This correlation coefficient, which we call "quality coefficient", should be minimal when the recording is correctly compensated. Fig. 8B shows in this recording how the compensation $L^p$ error varies when the estimated electrode Re and neuron resistance R are varied. The lowest error value is achieved with $R_e$ = 103 MΩ. Fig. 8C shows how the quality coefficient varies in the same recording when $R_e$ and R are varied. The lowest value is achieved with $R_e$ = 95 MΩ. These two panels confirm that these two error criteria are different in nature: the $L^p$ criterion is strongly modulated by the total resistance (electrode+neuron), while the quality coefficient mostly depends on the electrode resistance. For this specific recording, we may conclude that the estimation of $R_e$ should be correct within about 10 %. Note that this method based on the quality coefficient is also not perfect, because it implicitly assumes that the neuron's resistance is zero at spike peak, which of course is not exactly true, especially in neurons with small somatic spikes.

*Dendrites*

One important difficulty with all single-electrode compensation methods, including the present one, is that the presence of dendrites may contribute a fast component in the neuron's response to injected currents, potentially at the same timescale as the electrode response. With a single electrode, there is no principled way to distinguish between the two contributions, which means that an electrode compensation method may subtract both the electrode voltage and the dendritic response. In (Brette et al., 2008), it was shown in a multicompartmental model of a pyramidal cell that the dendritic contribution was not large enough to degrade the quality of recordings compensated with AEC. Here we simulated a pyramidal neuron model with two

compartments representing the soma and dendrites (Wang, 1998), with a filtered noisy current injected at the soma and an electrode model ($R_e$=200 MΩ and $\tau_e$=0.2 ms). The recording was compensated as previously, that is, the model used in the compensation procedure did not include a dendritic component (Fig. 9A). As is seen on Fig. 9A, the compensated recording is still very accurate (estimated $R_e$ was 171 MΩ). We then modified the neuron model used for the compensation procedure to include a dendritic compartment (electrical circuit shown on Fig. 9B). This improved the estimation of $R_e$ (192 MΩ). However, we should caution that there is no guarantee that adding a dendritic compartment in the compensation model will always improve the accuracy, because it may depend on the neuron's morphology, for example.

It could be that in other recordings (e.g. different cell morphologies), the dendritic component is more important, which could degrade the quality of compensation. However, as we noted, this problem is not worse than with any other single-electrode compensation method. In fact, to be more precise, dendritic and electrode responses are indistinguishable for any method based on the linear response of the circuit (neuron+electrode). This includes the present method, bridge, and discontinuous current clamp (DCC). But the independent control based on spike peaks that we presented above (Fig. 8) is in fact based on the nonlinear response of the neuron. Therefore it could also be used to test whether the compensation may be compromised by dendritic components.

*Application: spike threshold in vitro*

We finish with an application of this technique to the measurement of the spike threshold (more precisely, spike onset) in response to fluctuating currents in neurons of the cochlear nucleus. *In vivo*, the spike threshold in many areas shows significant variability. It is negatively correlated with preceding depolarization slope (Azouz et Gray, 2003; Wilent et Contreras, 2005) and with the preceding interspike interval (Henze et Buzsáki, 2001) (see (Platkiewicz et Brette, 2010a) for a more exhaustive overview). These properties have also been seen in cortical neurons *in vitro* in response to fluctuating conductances, using the dynamic clamp technique (Polavieja et al., 2005). In Fig. 10 we show similar results in a stellate cell of the cochlear nucleus, using current clamp injection of a fluctuating current (filtered noise with time constant 2 ms). This corresponds to the type of cell modeled in Fig. 3. One difficulty is that these cells tend to have short membrane time constants (about 5 ms in this cell), and therefore separating the electrode from the neuron response is more challenging.

Fig. 10A shows the compensated recording. Spike onsets (black dots) were measured according to a criterion on the first derivative of the membrane potential (dV/dt = 1 V/s). In this recording, the spike threshold distribution spanned a range of about 12 mV, with standard deviation σ = 2.1 mV, which is comparable to *in vivo* measurements in the cortex (Azouz et Gray, 2003; Wilent et Contreras, 2005) and in the inferior colliculus, another subcortical auditory structure (Peña et Konishi, 2002). This variability appeared higher in the uncompensated recording (σ = 2.9 mV), but also when bridge balance was used (σ = 2.6 mV), using the resistance value obtained by our method ($R_e$ = 45 MΩ). In addition, in both the uncompensated recording and the bridge compensated trace, there was a small inverse correlation between spike threshold and preceding depolarization slope (Fig. 10B,C; slope of the linear regression: -8 ms and -11.4 ms). This correlation was stronger when our compensation method was used (Fig. 10D; slope -18.2

ms). Thus, with our compensation method, the inverse correlation was stronger while the variability in spike threshold was smaller, which suggests that this stronger correlation is indeed the result of a more accurate estimation of spike threshold.

As a complementary test, we simulated a recording with a neuron model exhibiting a dynamic spike threshold (Fig. 10E). We used a simplified single-compartment model, in which the value of the spike threshold is explicitly known (Platkiewicz et Brette, 2010a, 2011a) (dashed curve in Fig. 10E). In the uncompensated recording, the spike threshold cannot be correctly measured (Fig. 10F), while it is correctly estimated in the compensated recording (Fig. 10G, note the different vertical scale).

## Discussion

We have a proposed a new method to correct the electrode bias in single-electrode current-clamp recordings. As with active electrode compensation (AEC) (Brette et al., 2008), the principle is to fit a model of the measurements, that includes both the electrode and the neuron, and to subtract the predicted electrode voltage. The main difference is that it does not require any preliminary calibration, and it still works when electrode properties change during the course of the recording (on a slow timescale). In addition, thanks to a special error criterion, the estimation procedure is not very degraded by action potentials and other nonlinearities. We have also proposed a method to reliability detect spikes, and an independent quality control based on analyzing spike peaks.

There are limitations, many of which are shared by other compensation methods. First, the electrode must be linear. This is a critical point, discussed in (Brette et al., 2008), and it may not always be satisfied. Unfortunately, no compensation method can solve this issue, because when the electrode is nonlinear, the injected current is also distorted (Purves, 1981). However, with our technique, we can track the temporal changes in electrode properties and possibly detect electrode nonlinearities (which would mean that electrode properties vary with the mean injected current). In fact, it is possible in principle to incorporate nonlinearities in the electrode model, but this would require to have a precise model, which is not available at this time. Second, the technique only corrects the measured potential, but not the injected current, which is still filtered by the electrode. Therefore, it is still useful to use the capacitance neutralization circuit on the amplifier, so as to minimize the electrode time constant (this is a feedback circuit, which corrects the current rather than the potential). This issue is also present in double-electrode recordings. Third, although in principle the electrode and neuron timescales do not need to be well separated, in practice it may be difficult to distinguish between neuron and electrode components that are on a similar timescale, for example fast dendritic components and electrode response. This issue is present with all single-electrode compensation techniques, which is another reason to use capacitance neutralization on the amplifier.

Another, more specific, issue is the choice of the neuron and electrode models. In the experiments shown in this paper, a simple RC circuit for each element (neuron and electrode) seemed sufficient to correct the recordings. We should note that the capacitance neutralization circuit was used in these recordings (although not fully), and therefore the residual capacitance was compensated (which could be distributed along the wall of the electrode). However, it might

not be sufficient in other cases. It is not a problem in itself, since it is straightforward to change the model to be optimized (in our software tool, this only means entering different equations for the model). For example, one could consider a more complex electrode model, with two resistors and two capacitors. These more complex models could be used when the quality of the fit is poor, or when there is a large temporal variability in estimated electrode properties.

This technique may be extended in several ways. First, although we only applied it to current-clamp recordings, it could be used in the dynamic clamp (Prinz et al., 2004) or even voltage clamp mode (implemented e.g. as a dynamic clamp with high gain). However, since in these modes the current depends in real time on the estimated membrane potential, the electrode compensation cannot be done offline and therefore requires preliminary calibration. One possible advantage over other techniques such as AEC is that it is more robust to neuronal nonlinearities (e.g. action potentials). This property may also make it more appropriate for *in vivo* recordings. Finally, we suggest that this technique could be used to fit neuron models to intracellular recordings (Jolivet et al., 2008; Gerstner et Naud, 2009; Rossant et al., 2011b). The current strategy is in two stages: first compensate the recordings (e.g. with bridge balance), then fit a neuron model to the compensated trace. Instead, we suggest that a better strategy is to directly fit a model of the full experimental setup, including the neuron and the electrode, to the uncompensated recordings.

## Acknowledgments

We thank Jean-François Léger for providing us with an *in vivo* intracellular recording of a prefrontal cortical neuron. This work was supported by the European Research Council (ERC StG 240132) and by the Swedish Research Council (grant no. 80326601).

## Appendix

**Model simulation with a linear filter.** When the model of the neuron and the electrode is linear, it can be efficiently simulated using a linear filter. More specifically, let us write the model equations as $\frac{d\mathbf{Y}}{dt}(t) = \mathbf{M}(\mathbf{Y}(t) - \mathbf{B}) + \mathbf{X}(t)$, where **Y** is a d-dimensional vector, **M** a d*d matrix, **B** is a d-dimensional vector, and $\mathbf{X}(t) = {}^t(x(t), 0, \ldots, 0)$, where x(t) is the fluctuating input current. In general, the linear model can be written under this form as soon as the matrix **M** is invertible. Assuming that the input current is sampled at frequency f=1/dt, we can numerically solve this equation by simulating the following discrete-time linear system: $\mathbf{Y}_{n+1} = \mathbf{A}\mathbf{Y}_n + \mathbf{X}_n$, where $\mathbf{A} = \exp(\mathbf{M} \cdot dt)$ and we applied the following change of variables: $\mathbf{Y} \leftarrow \mathbf{Y} - \mathbf{B}$. This system can be solved using a linear filter: $y_n = \sum_{k=0}^{d} b_k x_{n-k} - \sum_{k=1}^{d} a_k y_{n-k}$, where $y_n = \mathbf{Y}_n[i]$ and $x_n = x(n \cdot dt)dt$, and $i$ is the index of the variable to be simulated (typically, neuron and electrode potential). The values $a_k$ can be obtained by computing the characteristic polynomial of the matrix **A**, $P_A(X) = \det(X \cdot Id - \mathbf{A}) = \sum_{k=0}^{d} a_k X^{d-k}$. The values $b_k$ are obtained with

$b_k = T_k[i,0]$, where $T_k = \sum_{l=0}^{k} a_{k-l}\mathbf{A}^l$.

We give an outline of the proof here. We start from the Cayley-Hamilton theorem, which states that $P_A(\mathbf{A}) = 0$. We multiply this equation by $\mathbf{Y}_{n-d}$: $\sum_{k=0}^{d} a_{d-k}\mathbf{A}^k\mathbf{Y}_{n-d} = 0$. We then calculate $\mathbf{A}^k\mathbf{Y}_{n-d}$ by induction:

$$\mathbf{A}^k\mathbf{Y}_{n-d} = \mathbf{Y}_{n-d+k} - \sum_{p=1}^{k} \mathbf{A}^{k-p}\mathbf{X}_{n-d+p}$$

and we substitute it in the equation above, which gives:

$$0 = \sum_{k=0}^{d} a_{d-k}\mathbf{Y}_{n-d+k} - \sum_{k=0}^{d} a_{d-k} \sum_{p=1}^{k} \mathbf{A}^{k-p}\mathbf{X}_{n-d+p}$$

We then obtain the desired result by looking at coordinate *i*.

Using this technique, electrode compensation is very fast (close to real time with sampling rate 10 kHz), even though we implemented it in Python, an interpreted language.

## References


**Anderson J, Carandini M, Ferster D**. Orientation tuning of input conductance, excitation, and inhibition in cat primary visual cortex. *J neurophysiol* 84: 909, 2000.

**Angelo K, London M, Christensen SR, Häusser M**. Local and Global Effects of Ih Distribution in Dendrites of Mammalian Neurons. *The Journal of Neuroscience* 27: 8643 -8653, 2007.

**Azouz R, Gray CM**. Adaptive coincidence detection and dynamic gain control in visual cortical neurons in vivo. *Neuron* 37: 513–523, 2003.

**Brette R, Destexhe A**. Intracellular recording. In: *Handbook of neural activity measurement*. Cambridge University Press, 2012.

**Brette R, Piwkowska Z, Monier C, Rudolph-Lilith M, Fournier J, Levy M, Frégnac Y, Bal T, Destexhe A**. High-resolution intracellular recordings using a real-time computational model of the electrode. *Neuron* 59: 379-91, 2008.

**Cao X-J, Oertel D**. The magnitudes of hyperpolarization-activated and low-voltage-activated potassium currents co-vary in neurons of the ventral cochlear nucleus. *J. Neurophysiol.* 106: 630-640, 2011.

**Davie JT, Kole MHP, Letzkus JJ, Rancz EA, Spruston N, Stuart GJ, Hausser M**. Dendritic patch-clamp recording. *Nat. Protocols* 1: 1235-1247, 2006.

**Fourcaud-Trocme N, Hansel D, van Vreeswijk C, Brunel N**. How spike generation mechanisms determine the neuronal response to fluctuating inputs. *J neurosci* 23: 11628-40, 2003.

**Fujino K, Oertel D**. Cholinergic modulation of stellate cells in the mammalian ventral cochlear nucleus. *J. Neurosci.* 21: 7372-7383, 2001.

**Gerstner W, Naud R**. How Good Are Neuron Models? *Science* 326: 379-380, 2009.

**Goodman DFM, Brette R**. The Brian simulator. *Front Neurosci* 3: 192-197, 2009.

**Henze DA, Buzsáki G**. Action potential threshold of hippocampal pyramidal cells in vivo is increased by recent spiking activity. *Neuroscience* 105: 121–130, 2001.

**Jolivet R, Schürmann F, Berger TK, Naud R, Gerstner W, Roth A**. The quantitative single-neuron modeling competition. *Biol Cybern* 99: 417-426, 2008.

**Léger J-F, Stern EA, Aertsen A, Heck D**. Synaptic integration in rat frontal cortex shaped by network activity. *J. Neurophysiol.* 93: 281-293, 2005.

**Peña JL, Konishi M**. From Postsynaptic Potentials to Spikes in the Genesis of Auditory Spatial Receptive Fields. *The Journal of Neuroscience* 22: 5652 -5658, 2002.

**Platkiewicz J, Brette R**. A threshold equation for action potential initiation. *PLoS Comput. Biol* 6: e1000850, 2010a.

**Platkiewicz J, Brette R**. A Threshold Equation for Action Potential Initiation. *PLoS Computational Biology* 6: e1000850, 2010b.

**Platkiewicz J, Brette R**. Impact of fast sodium channel inactivation on spike threshold dynamics and synaptic integration. *PLoS Comput. Biol.* 7: e1001129, 2011a.

**Platkiewicz J, Brette R**. Impact of Fast Sodium Channel Inactivation on Spike Threshold Dynamics and Synaptic Integration. *PLoS Computational Biology* 7: e1001129, 2011b.

**Polavieja GG de, Harsch A, Kleppe I, Robinson HPC, Juusola M**. Stimulus history reliably shapes action potential waveforms of cortical neurons. *J Neurosci* 25: 5657–5665, 2005.

**Prinz AA, Abbott LF, Marder E**. The dynamic clamp comes of age. *Trends Neurosci* 27: 218, 2004.

**Purves RD**. *Microelectrode methods for intracellular recording and ionophoresis*. Academic Press New York, 1981.

**Rossant C, Fontaine B, Goodman DFM**. Playdoh: A lightweight Python library for distributed computing and optimisation. *Journal of Computational Science* , 2011a.

**Rossant C, Goodman DFM, Fontaine B, Platkiewicz J, Magnusson AK, Brette R**. Fitting Neuron Models to Spike Trains. *Front Neurosci* 5, 2011b.

**Rossant C, Leijon S, Magnusson AK, Brette R**. Sensitivity of noisy neurons to coincident inputs. *Journal of Neuroscience* In press, 2011c.

**Rothman JS, Manis PB**. The roles potassium currents play in regulating the electrical activity of ventral cochlear nucleus neurons. *J. Neurophysiol* 89: 3097-3113, 2003.

571 **Shu Y, Duque A, Yu Y, Haider B, McCormick DA**. Properties of Action-Potential Initiation in
572 Neocortical Pyramidal Cells: Evidence From Whole Cell Axon Recordings. *Journal of*
573 *Neurophysiology* 97: 746 -760, 2007.

574 **Wang X-J**. Calcium Coding and Adaptive Temporal Computation in Cortical Pyramidal Neurons. *J*
575 *Neurophysiol* 79: 1549-1566, 1998.

576 **Wehr M, Zador AM**. Balanced inhibition underlies tuning and sharpens spike timing in auditory
577 cortex. *Nature* 426: 442, 2003.

578 **Wilent WB, Contreras D**. Stimulus-dependent changes in spike threshold enhance feature
579 selectivity in rat barrel cortex neurons. *J Neurosci* 25: 2983–2991, 2005.

580

581

# Figure legends

**Figure 1.** Bridge and dynamic electrode compensation methods illustrated on a patch clamp recording in a pyramidal neuron from mouse auditory cortex. Top: injected current, starting with a current step for calibrating the bridge compensation method (left), and followed by a fluctuating current with fast transients (current B, right). Middle: bridge compensated membrane potential. Bottom: compensated trace using our technique.

**Figure 2.** The calibration-free electrode compensation technique. **A**. Overview of the technique. An input current is injected into a real neuron during a current clamp *in vitro* recording (top). The raw trace recorded by the electrode (gray) includes the responses of both the neuron and the electrode. Simultaneously, the current is injected into a linear (non-spiking) model of the neuron and electrode (bottom). The model parameters are adjusted by an optimization procedure so as to minimize the $L^p$ error (see text) between the model trace (black) and the raw trace (gray). The model is then used to predict the electrode response and subtract it from the raw trace, yielding the compensated trace. **B**. Compensation example. Left: raw trace (gray, filtered noise current) and full model trace (black). Right: compensated trace. **C**. Compensation of large EPSPs and action potentials using the mean squared error (p = 2). Left: raw (gray) and model (black) traces on a current with fast and large EPSCs (current B). The inset shows a zoom on an EPSP followed by an action potential: the model overestimates the EPSP because of the spike. Right: the compensated trace, showing distorted EPSPs and action potentials. The histogram of the differences between raw trace and optimized model trace (right) peaks below 0 mV because of the long positive tail due to action potentials. **D**. Same as C but with p = 0.5. This error criterion gives less weight to outliers such as action potentials, leading to a better estimation of the membrane potential.

**Figure 3**. Test of the electrode compensation method in a biophysical model of a cochlear nucleus neuron (Rothman et Manis, 2003) (resistance ~500 MΩ, time constant ~5 ms), with a non-ideal electrode (resistance $R_e$ = 50-500 MΩ, time constant $\tau_e$ = 0.1 ms). **A**. Top: a 1s fluctuating current with large and fast transients (set 3) is injected into the biophysical model ($R_e$ = 500 MΩ). Middle: raw (gray) and fitted model (black) traces using our compensation technique (p=0.5). The fitting procedure finds $R_e$ = 480 MΩ and $\tau_e$ =0.1 ms. Bottom: compensated trace (black) and biophysical neuron model trace (dashed gray), showing a perfect fit (inset). **B**. Scatter plot of the model and fitted electrode resistance values, using three different 1s currents (o: set 1, +: set 2, x: set 3, see Methods) and four different electrode resistance values ($R_e$ = 50 MΩ, 100 MΩ, 200 MΩ, 500 MΩ). **C**. Electrode and membrane resistance values found by the compensation technique when the actual resistance is $R_e$ = 100 MΩ (dashed line) as a function of p (current from set 1).

**Figure 4**. Test of the compensation method on real data. **A**. A fluctuating current (current B) is injected into a neuron of the mouse auditory cortex during a patch clamp experiment. Top: raw recorded trace. Bottom: compensated trace. **B**. A 590s long fluctuating current (current A, mean 10 pA, standard deviation 30 pA) is injected into a neuron. The trace is divided in 1 s windows, and the fitting procedure is applied independently on each window. Top: estimated neuron resistance as a function of time. Bottom: estimated electrode resistance as a function of time. Recordings at times 1 and 2 are shown in C. **C**. Raw (gray) and compensated (black) traces at times 1 (left, $R_e$ = 33 MΩ) and 2 (top right, $R_e$ = 81 MΩ). Bottom right: same as above but using

the electrode resistance obtained at time 1 (Re = 33 MΩ).

**Figure 5**. Robustness of the compensation method to changes in neuron or electrode resistance. **A**. Estimated neuron resistance (dots) and electrode resistance (crosses) in a simulated recording with a varying electrode resistance. The Rothman & Manis neuron model (type 1c) and an electrode model are simulated with a 20 s filtered noise current. After 10 s, the electrode resistance is increased abruptly from 100 MΩ to 300 MΩ during the last 10 seconds (dashed step: actual value of $R_e$). **B**. Estimated neuron and electrode resistance in an *in vitro* recording with an Ih blocker. Filtered noise current is injected into a bushy cell during 8 min. The Ih blocker ZD788 (10μM) is applied to the bath during the second half of the stimulation, which increases neuron resistance. Dotted lines are linear regressions of the estimated neuron resistance in the two parts of the experiment.

**Figure 6**. A method for spike detection in an intracellular recording. **A**. A 30 s compensated recorded trace of a pyramidal cell in vitro, seen in phase space ( dV/dt vs. V), for a filtered noise injected at the soma. Large cycles correspond to spikes. **B**. Distribution of voltage values measured when the trajectory in phase space (A) crosses the horizontal dashed line dV/dt = 0 (local maxima and minima). Two modes appears, corresponding to fluctuations (left) and to spike peaks (right). An optimal separatrix between the two modes is calculated (dashed vertical line). The two modes in the histogram are fitted to Gaussian distributions, which are used to quantify spike detection quality. **C**. An example of spikes detected with this method on a compensated trace (solid line). The dashed line indicates the decision threshold, and detected spike peaks are shown with filled circles.

**Figure 7**. Quality and stability of electrode compensation. **A**. Estimated neuron (o) and electrode (x) resistance (line: actual electrode resistance of the model) as a function of time, on a simulated recording with an injected noisy current (filtered noise) (same model as in Fig. 3, $R_e$ = 200 MΩ). The mean firing rate was ~8 Hz. **B**. Action potential shapes. Top: spikes recorded *in vivo* in a neuron of the prefrontal cortex (Léger et al., 2005). On the right, the same spikes are shown in the phase plane (V, dV/dt) (see Methods). Middle: compensated spikes of a cortical neuron in response to a fluctuating current. Bottom: same as above but when the estimated electrode resistance is increased by 25%.

**Figure 8**. Control of electrode compensation using spike peaks. **A**. Illustration of the method. For each spike, a linear regression is performed on the compensated trace (top, black; uncompensated trace is in grey) in a temporal window from 10 ms to 2 ms before spike peak. We then compute the best linear prediction of the spike peak, given the two regression parameters (intercept and slope). The quality coefficient is defined as the Pearson correlation between the prediction error and the mean input current around spike peak (2 ms before to 1 ms after; grey horizontal line on the bottom trace). **B**. $L^p$ error between the model trace and the measured trace, as a function of the model neuron and electrode resistances, with all other parameters fixed at their optimal values. The parameter values giving minimum error are represented by the cross. **C**. Quality coefficient as a function of the model neuron and electrode resistances, with the best parameters represented by the cross.

**Figure 9**. Test of the method with a two-compartmental neuron model. **A**. A pyramidal neuron model with two compartments (soma and dendrite) and a linear electrode are simulated, with a filtered white noise injected current. The recorded trace (grey) is then compensated with our

method (p=0.5). The compensated trace (solid black) matches the neuron voltage (dotted), except for spikes that are filtered by the electrode. **B**. The same trace is compensated, but the compensation model now includes a dendritic current.

**Figure 10.** Spike threshold measurements in a stellate cell of the cochlear nucleus. **A.** Compensated voltage trace of a stellate cell in response to an injected fluctuating current. Spike thresholds are measured as the membrane potential when the first derivative exceeds 1 V/s (dots). **B.** Spike threshold as a function of depolarization rate in the 10 ms preceding each spike, when the trace is not compensated (dashed line: linear regression). **C**. Same relationship in the bridge compensated trace. **D**. Same relationship in the trace compensated with our method. **E**. Simulated recording with a neuron model with adaptive spike threshold and an electrode model ($R_e = 60M\Omega$ and $\tau_e = 0.6$ ms). The uncompensated recording is the solid grey curve, the compensated recording the solid black curve. The real membrane potential is shown in dotted grey but at this scale, it is only distinguishable after spikes. The dynamic spike threshold is the dashed black curve. **F**. Spike threshold measured at spike times in the uncompensated recording vs. actual spike threshold. **G**. Spike threshold measured at spike times in the compensated recording vs. actual spike threshold (note the different vertical scale).

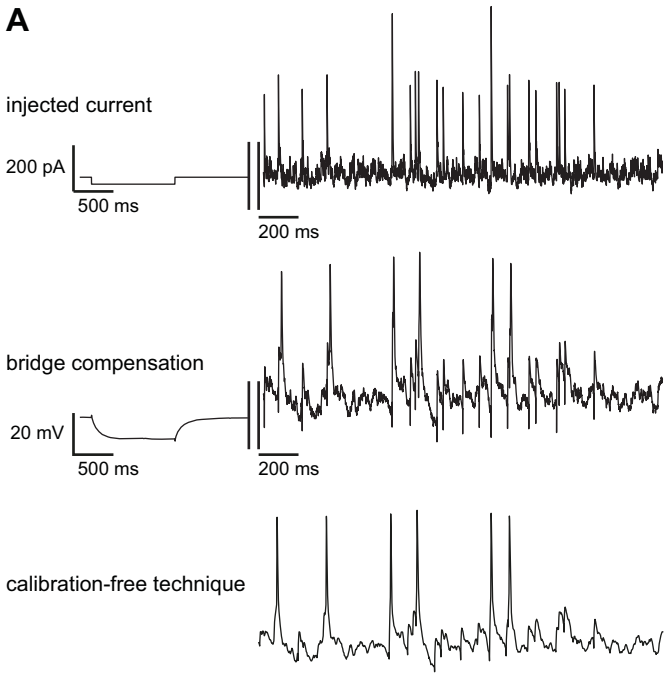
A
injected current
200 pA
500 ms
200 ms
bridge compensation
20 mV
500 ms
200 ms
calibration-free technique

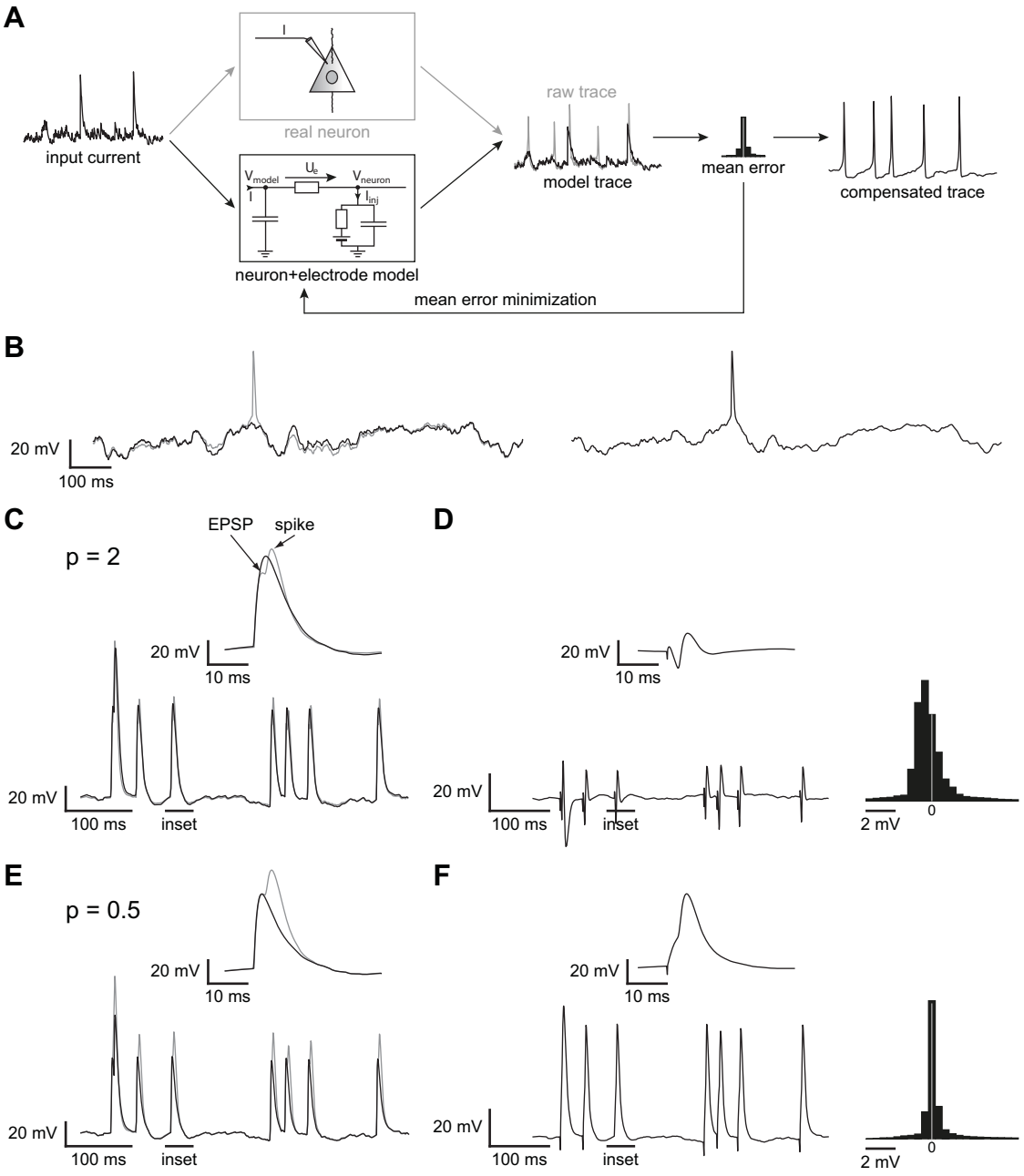
A
input current
real neuron
neuron+electrode model
raw trace
model trace
mean error
compensated trace
mean error minimization
B
20 mV
100 ms
C
p = 2
EPSP
spike
20 mV
10 ms
20 mV
100 ms
inset
D
20 mV
10 ms
20 mV
100 ms
inset
2 mV
0
E
p = 0.5
20 mV
10 ms
20 mV
100 ms
inset
F
20 mV
10 ms
20 mV
100 ms
inset
2 mV
0

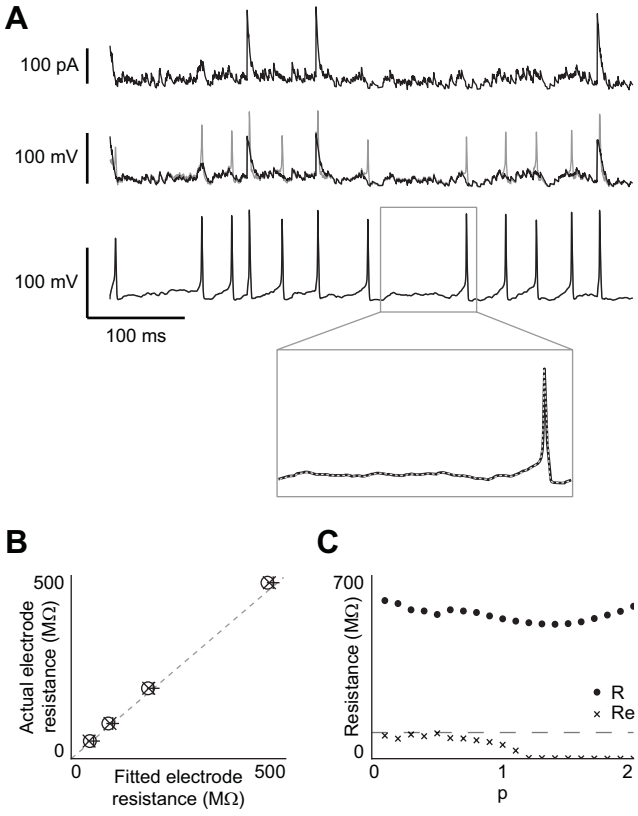
A
100 pA
100 mV
100 mV
100 ms
B
500
Actual electrode resistance (MΩ)
0
0
Fitted electrode resistance (MΩ)
500
C
700
Resistance (MΩ)
0
R
Re
0
1
2
p

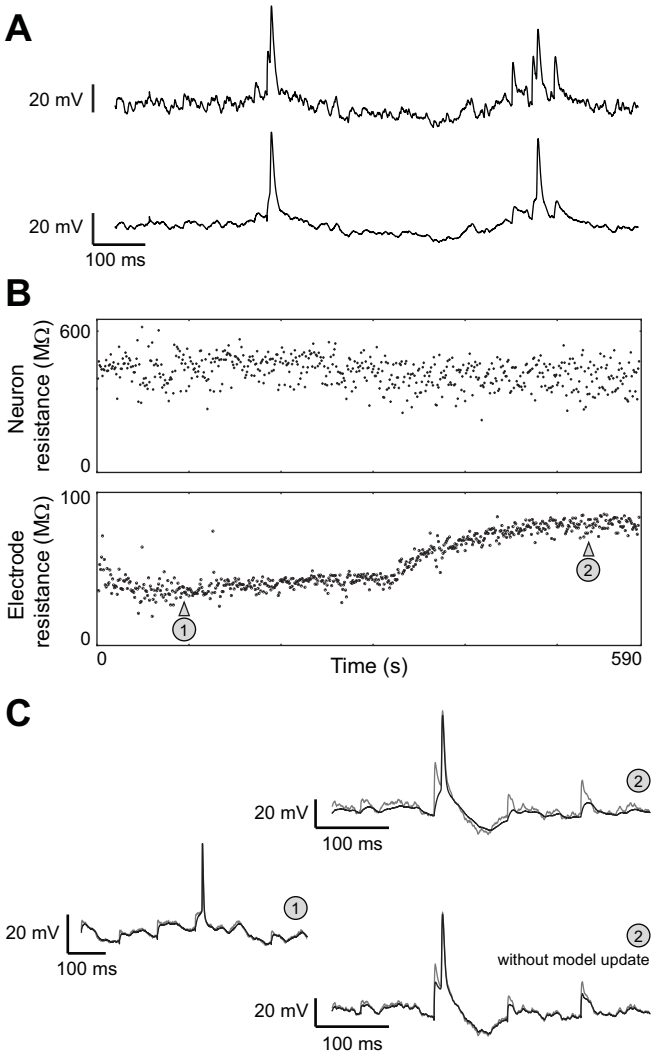
A
20 mV
20 mV
100 ms
B
Neuron resistance (MΩ)
600
0
Electrode resistance (MΩ)
100
0
1
2
0
Time (s)
590
C
20 mV
100 ms
1
20 mV
100 ms
2
2
without model update
20 mV
100 ms

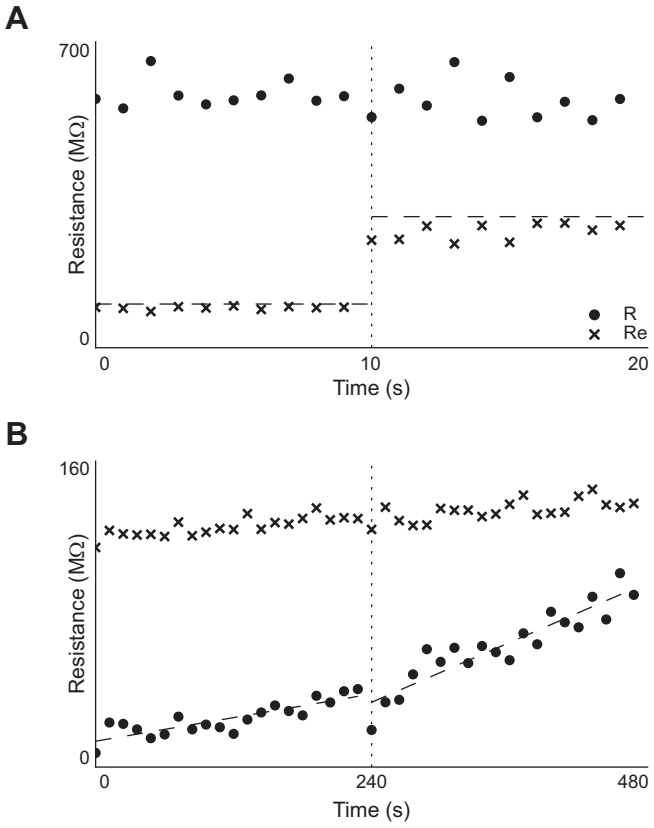
A
700
Resistance (MΩ)
0
0
10
20
Time (s)
R
Re
B
160
Resistance (MΩ)
0
0
240
480
Time (s)

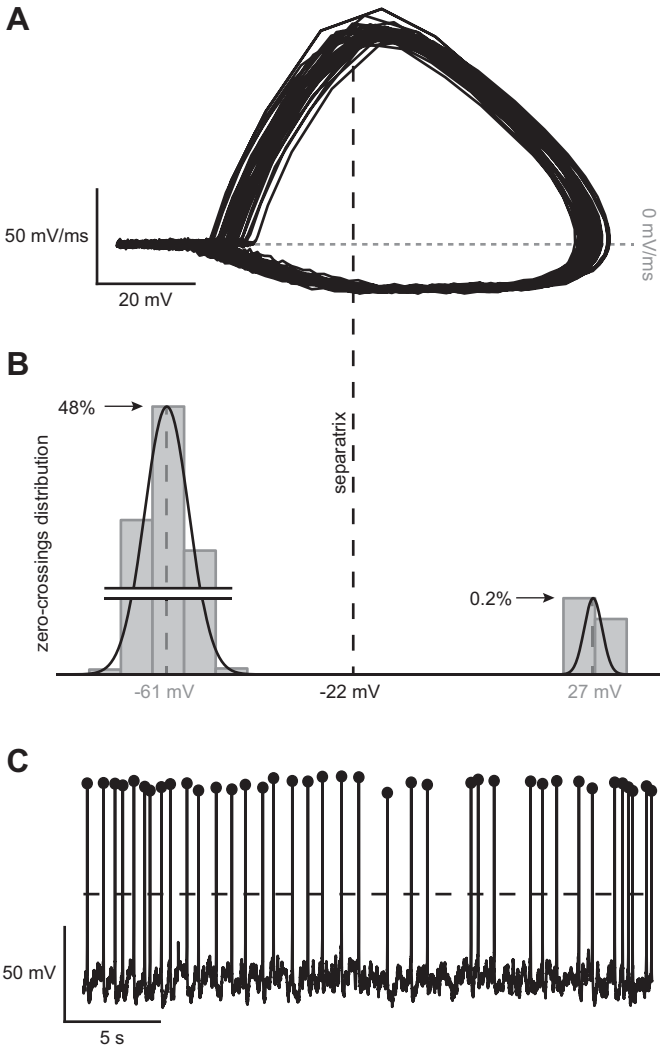
A
50 mV/ms
20 mV
0 mV/ms
B
48%
zero-crossings distribution
separatrix
0.2%
-61 mV
-22 mV
27 mV
C
50 mV
5 s

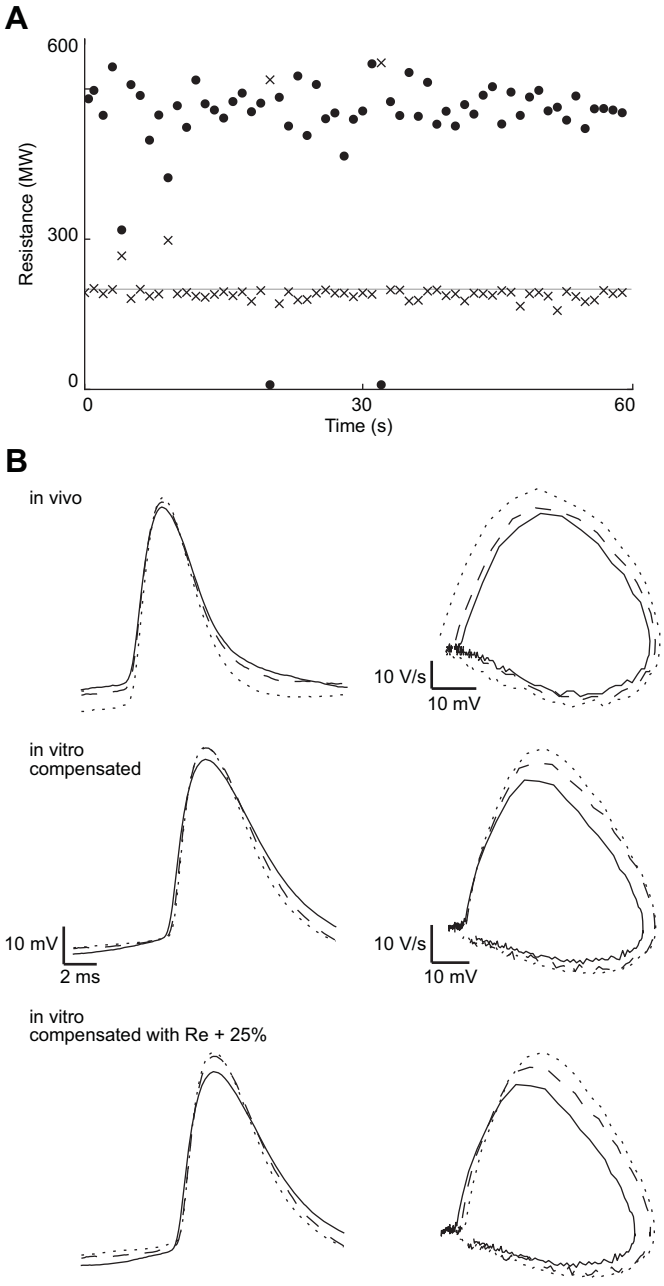
A
600
300
0
Resistance (MW)
0
30
60
Time (s)
B
in vivo
10 V/s
10 mV
in vitro
compensated
10 mV
2 ms
10 V/s
10 mV
in vitro
compensated with Re + 25%

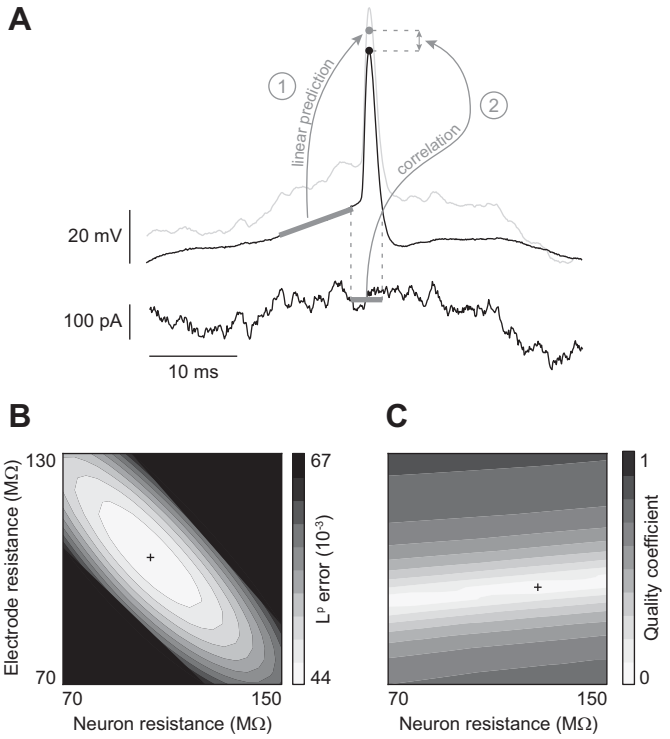
A
1
linear prediction
2
correlation
20 mV
100 pA
10 ms
B
130
70
Electrode resistance (MΩ)
70
150
Neuron resistance (MΩ)
67
44
L^p error (10^-3)
C
70
150
Neuron resistance (MΩ)
1
0
Quality coefficient

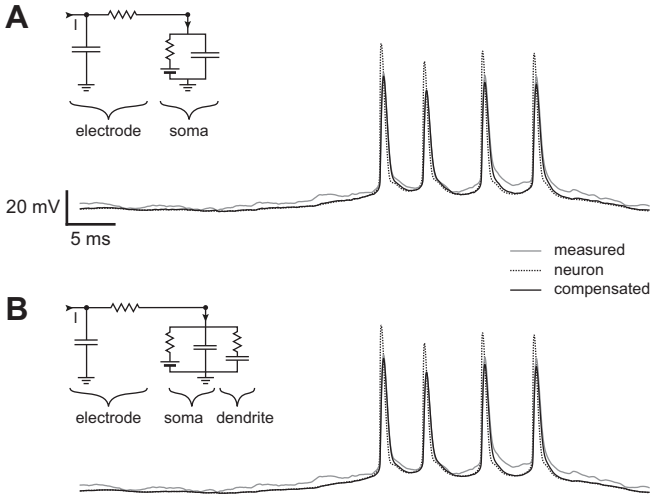
A
electrode
soma
20 mV
5 ms
measured
neuron
compensated
B
electrode
soma
dendrite

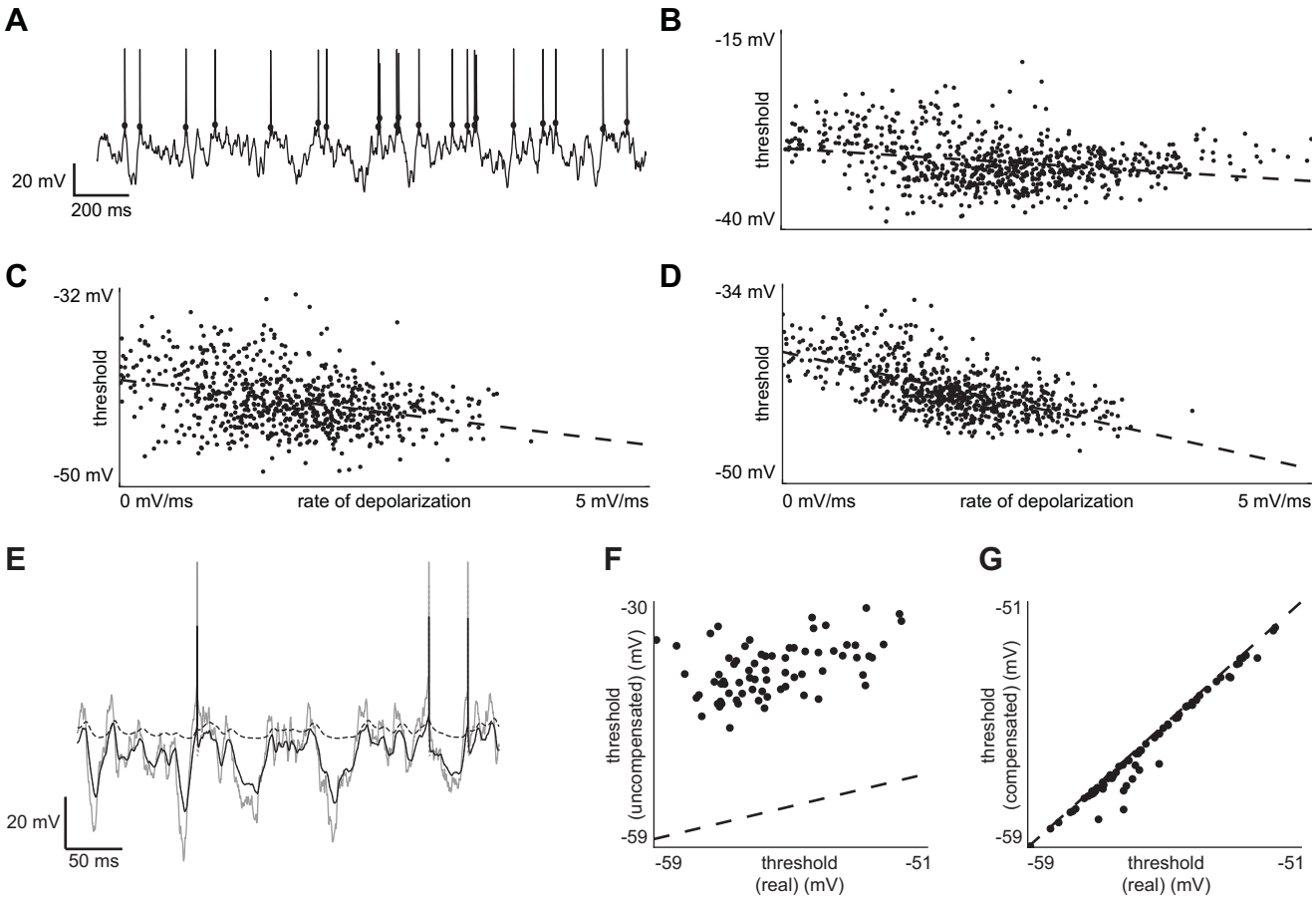
A
20 mV
200 ms
B
-15 mV
threshold
-40 mV
C
-32 mV
threshold
-50 mV
0 mV/ms
rate of depolarization
5 mV/ms
D
-34 mV
threshold
-50 mV
0 mV/ms
rate of depolarization
5 mV/ms
E
20 mV
50 ms
F
-30
threshold (uncompensated) (mV)
-59
-59
threshold (real) (mV)
-51
G
-51
threshold (compensated) (mV)
-59
-59
threshold (real) (mV)
-51